Universität Rostock Traditio et Innovatio

Analysis of Baltic Sea climate variability based on model data for the last 8000 years

Bachelor's thesis
written at the Institute of Physics
of the Faculty of Mathematics and Natural Sciences
of the University of Rostock

Marti Wolff, born 22nd October 1999 in Magdeburg

Supervisor and 1. Examiner : Prof. Dr. H. E. M. Meier, Leibniz Institute for Baltic Sea Research Warnemünde, Rostock
2. Examiner: Dr. F. Börgel, Leibniz Institute for Baltic Sea Research Warnemünde, Rostock

Rostock, 24th May 2023

https://doi.org/10.18453/rosdok_id00004903

Dieses Werk ist lizenziert unter einer
Creative Commons Namensnennung 4.0 International Lizenz.

Abstract

The Max Planck Institute Earth System Model MPI-ESM1.2 performed a global transient Holocene simulation spanning the period 6000 BCE to 1850 CE. The simulation only accounts for orbital and land-use forcing. Within the model data the climate of the Baltic Sea region, defined with a specific mask, was analysed. A systematic temperature shift yielding higher spring and lower summer temperatures was identified and attributed to changing northern hemisphere insolation. The Holocene Climate Optimum (HCO), the Medieval Climate Anomaly (MCA) and the Little Ice Age (LIA) were identified through temperature anomalies of about $\pm$0.2K and the prevailing climate analysed. Primarily during winter months the North Atlantic Oscillation (NAO) was found to influence the Baltic Sea region climate. This influence is characterized by correlation coefficients above 0.5 between the Baltic Sea region temperature and the Baltic Sea region precipitation as well as the NAO pressure difference. Substantial temperature anomalies during MCA fall and LIA spring coinciding with fluctuations of the NAO pressure difference were found.

Contents

1. Introduction **1**

2. Methods **5**

2.1. Model data 5

2.2. Data evaluation 6

2.2.1. Baltic Sea catchment area definition 6

2.2.2. Analysis strategy 7

2.2.3. NAO pressure difference dynamic calculation 10

3. Results **11**

4. Discussion and Conclusion **23**

A. Figures **29**

Bibliography **33**

Chapter 1.

Introduction

Studying how climates have changed in the past helps in understanding the fundamental mechanisms of natural climate variability. Applying this knowledge to climate models crucially improves their ability to predict future climate change. The reconstruction of past climate is often based on a combination of historical records of direct observations and proxy data such as tree rings, glacier ice and marine sediments and climate models [PAGES 2k Consortium, 2013]. Historical records and proxy data are limited and only provide information on specific aspects like temperature and wind on regional scales. Climate models on the other hand are able to produce a thorough and complete picture of global past climate in contrast to the reconstructions, which is why they play an essential role in paleoclimate reconstruction [Ludwig et al., 2018]. Modern paleoclimate reconstructions such as Askjær et al. [2022] use a combination of recorded and reconstructed data and climate models.

In this research the climate of the Baltic Sea region is analysed based on model data of the Earth System Model of the Max Planck Institute for Meteorology (MPI-ESM1.2) [Giorgetta et al., 2013] which performed a global transient Holocene simulation. The model uses the general circulation models GCMs, [e.g. Balaji et al., 2022] ECHAM6 [Stevens et al., 2013] for the atmospheric and MPI-OM [Jungclaus et al., 2013] for the ocean component in combination with the JSBACH land model [Reick et al., 2013]. Gutjahr et al. [2019] described the models adaption to higher horizontal resolutions and improved ocean physics in his research. The run analysed in this research only takes interactive vegetation and orbital forcing into account (SLO0043). A different MPI-ESM1.2 run performed by the Max-Planck-Institute for Meteorology included orbital forcing, spectral solar irradiance, greenhouse-gas concentrations, land-use changes, stratospheric volcanic aerosol distribution, and stratospheric ozone. The results are

used by Bader et al. [2020] who discovered a global cooling and warming mode during the Holocene and by Dallmeyer et al. [2020] who analysed the end of the African humid period.

Of course the MPI-ESM is not the first climate model. The ECHO-G coupled climate model used by Min et al. [2004] consists of the atmospheric component ECHAM4 and the ocean component HOPE-G and external forcing is fixed. The atmosphere–ocean general circulation model (AOGCM) of the Max-Planck-Institute for Meteorology [Jungclaus et al., 2006] was used as a prototype by the Intergovernmental Panel on Climate Change (IPCC) for their Fourth Assessment Report (AR4). It unites the ECHAM5 atmospheric component with the MPI-OM ocean component coupled by OASIS. Four years later the first ensemble simulations over the last 1200 years with an Earth system model including a full carbon cycle were done [Jungclaus et al., 2010]. The model included ECHAM5, MPI-OM, OASIS3 and the carbon cycle consisting of the ocean biogeochemistry model HAMOCC5 and the JSBACH land-surface model. The simulation accounted for solar, volcanic, orbital, greenhouse gas and aerosol forcing and land cover changes.

A good overview of state of the art transient Holocene simulations is given by Askjær et al. [2022]. Besides the MPI-ESM1.2 examined in this research used models include the AWI-Earth System Model 2 [Shi et al., 2020], the EC-Earth3 [Zhang et al., 2021], the HadCM3-M2.1d [Hopcroft and Valdes, 2021], the IPSL ESM [Braconnot et al., 2019] and the NNU 12k model [Sun et al., 2020]. All of the models can account for sea ice, vegetation, land-surface, orbital forcing and greenhouse gases. Few comprehend ice-sheets, solar irradiance and land use forcing. But only the HadCM3-M2.1d and the MPI-ESM1.2 are advanced enough to take volcanic forcing into account. Recent studies show that volcanic activity can be a strong driver of climate variability [Sigl et al., 2015], [Lin et al., 2022] which underlines the importance of the inclusion of volcanic forcing in climate models. Mann et al. [2021] recently concluded that the Atlantic Multidecadal Oscillation which constantly influences the Baltic Sea [Börgel et al., 2018] is primarily forced by explosive volcanism.

As done with the inclusion of volcanoes, climate models are constantly being improved and developed further. The Coupled Model Intercomparison Project (CMIP) [Eyring et al., 2016] is an international effort to compare and evaluate climate models from around the world. A main part of the project is the Paleoclimate Modelling Intercomparison Project PMIP [Kageyama et al., 2018] which compares modelled pale-

oclimate with reconstructions based on physical, geological or chemical records. This comparison is carried out for five different periods, one of them being the mid Holocene spanning the last 6 ka [Otto-Bliesner et al., 2017].
All of the climate models mentioned above are global models. The global scale of the models causes the need of high computing power and a coarse resolution compared to regional climate models. Using the latter can be beneficial especially over areas with a complex surface structure and at modelling hydrological processes [Ludwig et al., 2018]. Attempts are already made modelling the climate of the Baltic Sea region with regional climate models [e.g. Schimanke et al., 2012, Kjellström and Ruosteenoja, 2007].

There are two quasi-stationary sea level pressure systems in the Northern Atlantic: the Icelandic Low located near Iceland and the Azores High located around the Azores off the Portuguese coast. The pressure gradient between them is not constant but rather oscillates on decadal time frames. The oscillation is often quantified by the NAO index which takes on positive or negative values depending on the pressure difference [e.g. Börgel, 2020]. The NAO has a major influence on wind fields and thus heat and precipitation flux over the central and eastern North Atlantic [Hurrell, 1995]. This effect continues further to the NAO not only directly influencing Northern Atlantic climate but also having a major impact on Baltic Sea climate in winter [Lehmann et al., 2002, Schimanke et al., 2012].

A big part of studying paleoclimate is the investigation of longer periods of climate anomalies. Identifying their causes gives important insight into internal feedback mechanisms of the Earth's climate system. The three most researched global Holocene climate periods are the Holocene Climate Optimum (HCO), the Medieval Climate Anomaly (MCA) and the Little Ice Age (LIA). Warden et al. [2017] described the HCO in Europe as a period of higher temperatures starting about 6000 years ago and lasting for 1500 years based on sea surface temperature records from the Baltic Sea. The research reasons the cooling at the end of the HCO with a decrease in summer insolation. The European temperature reconstruction of the PAGES 2k Consortium [2013] found warmer temperatures from the 8th to 10th century while a colder climate prevailed from 1250 to 1850 CE highly coinciding with periods of volcanic-solar forcing. Mann et al. [2009] used proxy records and model reconstructions to date the MCA from 950 to 1250 CE and the LIA from 1400 to 1700 CE. They explain the development of the periods through the influence of large-scale processes, such as the NAO and El

Niño, which responded to solar insolation forcing. The research of Miller et al. [2012] concluded that the LIA was caused by volcanism and continued due to sea-ice/ocean feedbacks. Trouet et al. [2009] found a strong NAO+ mode dominating the European MCA and a weakening of that mode to be part of the transition to the LIA.

Within the framework of this research the climate periods HCO, MCA and LIA were identified and the interrelation between Baltic Sea region temperature and precipitation was analysed on a spatial and temporal scale for the model period and the climate periods. The NAO was characterized and the seasonal influence of the NAO pressure difference on the previous results was analysed.

The following chapter will give an overview of the model data and the used evaluation methods including a Baltic Sea catchment area mask. Afterwards the results for the climate periods, the temperature precipitation interrelation and the NAO influence are presented. They are furthermore discussed with regard to the findings of other researches and concluded. Further implications of the findings are presented.

Chapter 2.

Methods

2.1. Model data

This research evaluates model data of the Max Planck Institute for Meteorology Earth System Model MPI-ESM1.2 [Giorgetta et al., 2013]. The model performed a global transient Holocene paleoclimate simulation spanning the period of 6000 BCE to 1850 CE. Thus it only covers preindustrial times and doesn't account for human-made greenhouse gas emissions. The simulation employs the general circulation model ECHAM6 modeling the atmospheric component [Stevens et al., 2013], the JSBACH land model modeling soil and vegetation [Reick et al., 2013], the ocean general circulation model MPI-OM [Jungclaus et al., 2013] including a sea-ice model and the HAMOCC5 model for marine biogeochemistry, and the coupling program OASIS. A further explanation of the model composition is given in the paper of [Giorgetta et al., 2013]. This research investigates ECHAM6 data with a T63 resolution of 1.875° x 1.875° on 47 vertical levels.
Albeit the models ability to account for volcanic forcing the run investigated in this research only includes forcing through land use and orbital changes. The land use forcing is geared to Hurtt et al. [2011]. It starts at 850 CE and linearly builds up over a 1000 year period starting at 150 CE. The work of Berger [1978] regarding Earth's orbital elements is applied to quantify orbital forcing. It includes a decline in northern hemisphere summer and an incline in winter insolation over the model period. The model uses the proleptic Gregorian calendar.
The model data contains monthly values of the *2m temperature* (ECHAM6-Code 'var167'), the *total precipitation* ('var260') as a sum of *large-scale precipitation* ('var142') and *convective precipitation* ('var143'), and the *mean sea level pressure* ('var151')

amongst others. These three variables are analysed within this research. They will be referred to as temperature, precipitation and NAO pressure in the following. The model data was accessed in netcdf-files using Jupyter Notebook software with Python 3 as programming language. The data of each variable consisted of values for three coordinates, time with a length of 94200, longitude with a length of 192 and latitude with a length of 96 values.

2.2. Data evaluation

2.2.1. Baltic Sea catchment area definition

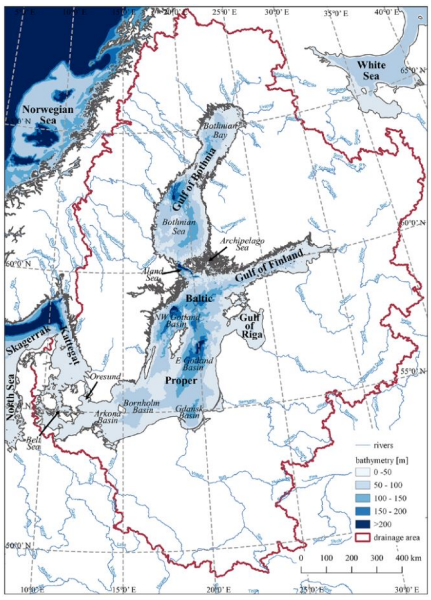

Figure 2.1: The Baltic Sea catchment area. The red line marks the boundary up to which the precipitation runs into the Baltic Sea. Source: [Kuliński et al., 2022].

As the ECHAM6 is a global circulation model the model data contains values for the whole Earth. There are mainly two different ways to select the wanted Baltic Sea region characterized by the Baltic Sea catchment area (see Figure 2.1) which covers all freshwater inflows into the Baltic Sea out of the data.
The first and easier way is to define a longitude-latitude rectangle, for example from $9.6°E$ to $32°E$ and $52.4°N$ to $67.4°N$ [Börgel et al., 2018]. That way most of the catchment area is covered but it also contains some additional parts that are not part of the catchment area. During the data analysis for this research a second, more accurate

definition was used. A specific mask for the catchment area was designed. Rectangle and mask are shown in Figure 2.2. Note that the mask has a fairly different shape than the catchment area shown in Figure 2.1. This is due to the usage of different coordinate systems: Figure 2.1 shows the Baltic region in spherical coordinates looked at from above whereas Figure 2.2 shows the region with latitude and longitude as Cartesian coordinates. A comparison of mean temperature and precipitation of the regions characterized by the two methods reveals the mask region being about 0.82K warmer and receiving 0.035 mm/day (1.5% of model mean) less precipitation on average. The temporal development of these divergences between the two methods over the model period is shown in Figure A.1.

For an even more detailed inspection the catchment area can be divided into the three parts Baltic Sea, land north of 60°N and land south of 60°N. This subdivision allows the observation of differences between land and sea area as well as possible north-south gradients. A map of the three resulting masks is shown in Figure 2.3.

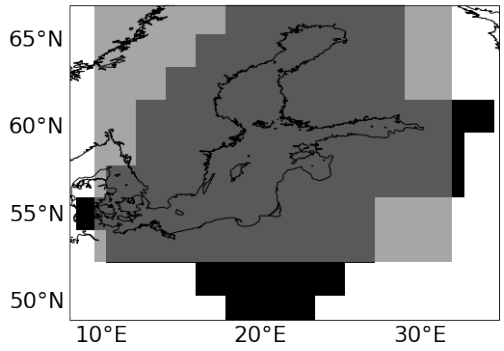

Figure 2.2: Comparison of longitude latitude rectangle from 9.6°E to 32°E and 52.4°N to 67.4°N (grey) and specific mask (black). The mask covers some areas that the rectangle doesn't, therefore it doesn't include other parts such as the top left corner which belongs to the Atlantic catchment area.

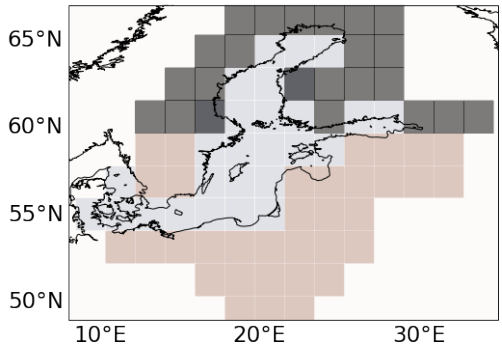

Figure 2.3: Subdivision of the Baltic Sea catchment area into the three parts Baltic Sea, land north of 60°N and land south of 60°N. Due to the grid point size of 1.875° x 1.875° some squares that are covered by water and land.

2.2.2. Analysis strategy

This research uses three main types of plots based on different statistical methods. The line plot shows temperature, precipitation or pressure as a function of the time,

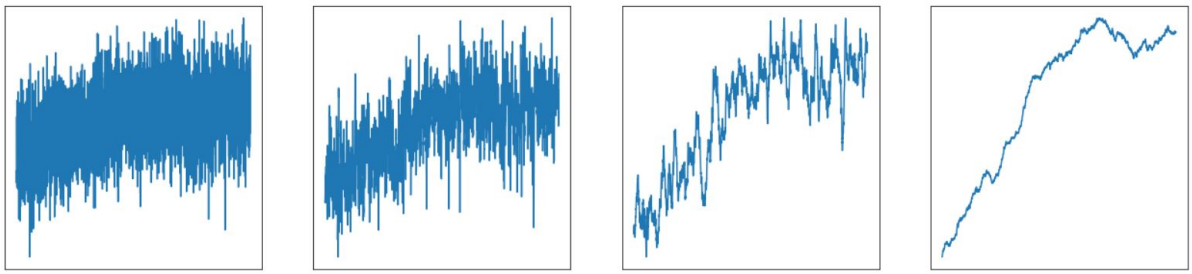

Figure 2.4: Exemplary Illustration of the effect of moving averages. This figure shows the same data set with different moving averages applied to. The data set has a length of 7850 years. From left to right the moving average length is 1, 10, 100 and 1000 years. A strong flattening of the curve is visible.

which is averaged over the Baltic region or one of the subdivisions shown in Figure 2.3. These variables are looked at through their annual average on the one hand, and on the other hand through seasonal averages. For spring the mean value of March, April and May is calculated for each year. June, July and August are summed up as summer; September, October and November as fall and December, January and February as winter. The research tries to find trends over time which is why it doesn't look at how the actual values develop over time but rather at the anomaly from the mean over a time frame. This perspective effectively only shifts the y-axis so that it doesn't influence any curve but puts it in a better perspective to the mean value laying at 0. Furthermore moving averages are used to flatten out the curves which helps to reduce noise so that some possible underlying effects might become visible. A moving average assigns each value the average of previous values and the value itself - for example the ten value moving average of the data point x_{19} is the average of the values of x_{10} to x_{19}. An illustration is shown in Figure 2.4. Without the use of moving averages trends would be considerably harder to detect and some shorter time scale effects might not be visible at all. Nonetheless moving averages also smear the data so that e.g. a 50 year long anomaly cannot be detected while applying a 500 year moving average to the data.

Map plots show the value of a variable for each grid point of the Baltic catchment area averaged over a certain time frame. This time frame can e.g. be the whole model period or a certain climate period. It is also possible to filter the data seasonally so that seasonal developments become visible in a spatial resolution. Similar to the line plots the map plots show the temperature and precipitation anomaly from the model period mean or the mean over a certain time period. That way local differences are resolved better and it is easier to detect whether an anomaly is positive or negative. Figure 2.5 shows three illustrative map plots of the Baltic Sea region.

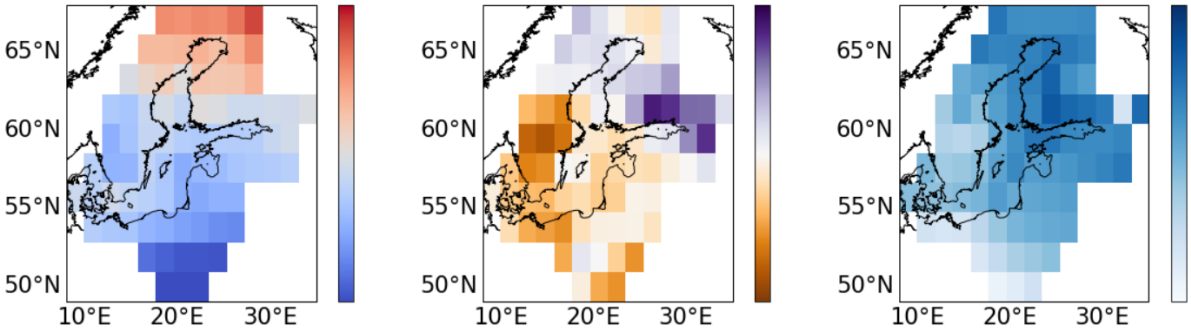

Figure 2.5: Three exemplary map plots of temperature and temperature anomaly (left), precipitation anomaly (middle) and total precipitation (right). The ability of this plot method to present spatial differences is obvious, the good resolution of a north to south temperature gradient and a west to east precipitation gradient are worth noting.

Seasonal cycle plots are an additional method to depict the data as shown in Figure 2.6. A variable is analysed during a specific time period and the mean value is calculated for each month. Applying this method to multiple time periods can visualize seasonal shifts in the variable between the viewed time periods. Additionally if e.g. the Baltic Sea region temperature over the model period is investigated, the temperature has to be averaged over the area first. Using a different mask, e.g. land north of 60° N reveals local differences in the seasonal cycles.

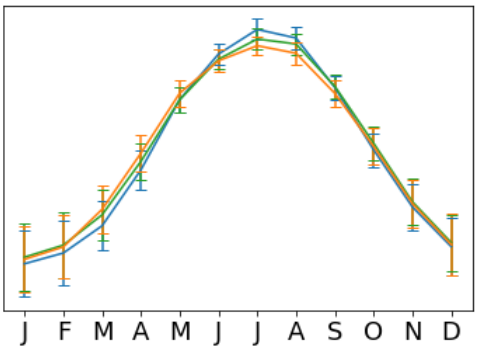

Figure 2.6: Illustration of a seasonal cycle plot. In this Figure the seasonal cycles of three different time slices are pictured. Note the seasonal shift from blue to orange to green. The error bars represent the standard deviation of the average value for each month.

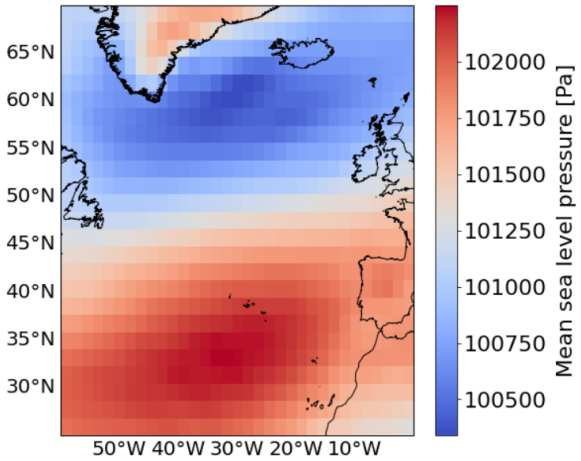

Figure 2.7: Mean sea level pressure over model period. The Icelandic Low and the Azores High are well recognizable. Both pressure areas are fairly spread out which reasons a dynamical calculation of the pressure difference.

2.2.3. NAO pressure difference dynamic calculation

The North Atlantic Oscillation is characterized by the pressure difference between Azores High and Icelandic Low. Their location varies spatially. The calculation of the difference between the pressure systems used in this research identifies the Icelandic Low pressure at a given time as the minimum mean sea level pressure from 55° N to 68° N and 24° W to 37° W and the Azores High pressure as the maximum mean sea level pressure from 27° N to 40° N and 26° W to 39° W. These borders were picked based on Figure 2.7 which shows the mean sea level pressure over the North Atlantic averaged over the model period. This dynamic approach allows a more accurate calculation of the NAO pressure compared to the use of fixated grid points such as Reykjavik and Lisbon for the pressure systems.

Chapter 3.

Results

At first the seasonal mean temperatures and precipitations of the Baltic Sea region were averaged over the whole model period and observed spatially. They are pictured in Figure 3.1 and 3.2 in the left columns. The temperatures are highest in summer and lowest in winter and in general getting higher going from North to South. Precipitation is highest in summer and lowest in spring. The map plots show that in spring and summer precipitation over the Baltic Sea is lower than over the surrounding land and the opposite in fall and winter. Calculating the seasonal mean values of the whole region on top of the temporal mean yields the values shown in Table 3.1.
If temperature and precipitation are not averaged over the model period but only over the Baltic Sea region instead, the middle columns of Figure 3.1 and 3.2 (100 year moving average (MA) applied) follow. The right columns of Figure 3.1 and 3.2 show temperature and precipitation change over the model period calculated as the 850 CE - 1850 CE mean subtracted from the 6000 BCE - 5000 BCE mean. The analysed region is getting warmer in spring and colder in summer, both developments most pronounced over land north of 60°N and least pronounced over the Baltic Sea. Also summers are becoming dryer over land and falls are becoming dryer in the southeast of the Baltic Sea region. For fall and winter temperature and spring and winter precipitation there is no systematic trend over the model period distinct.

Table 3.1.: Seasonal mean temperature and precipitation of the Baltic Sea region.

	Spring	Summer	Fall	Winter
Temperature [°C]	3.1	15.2	5.5	-5.1
Precipitation [mm/day]	1.9	2.8	2.5	2.0

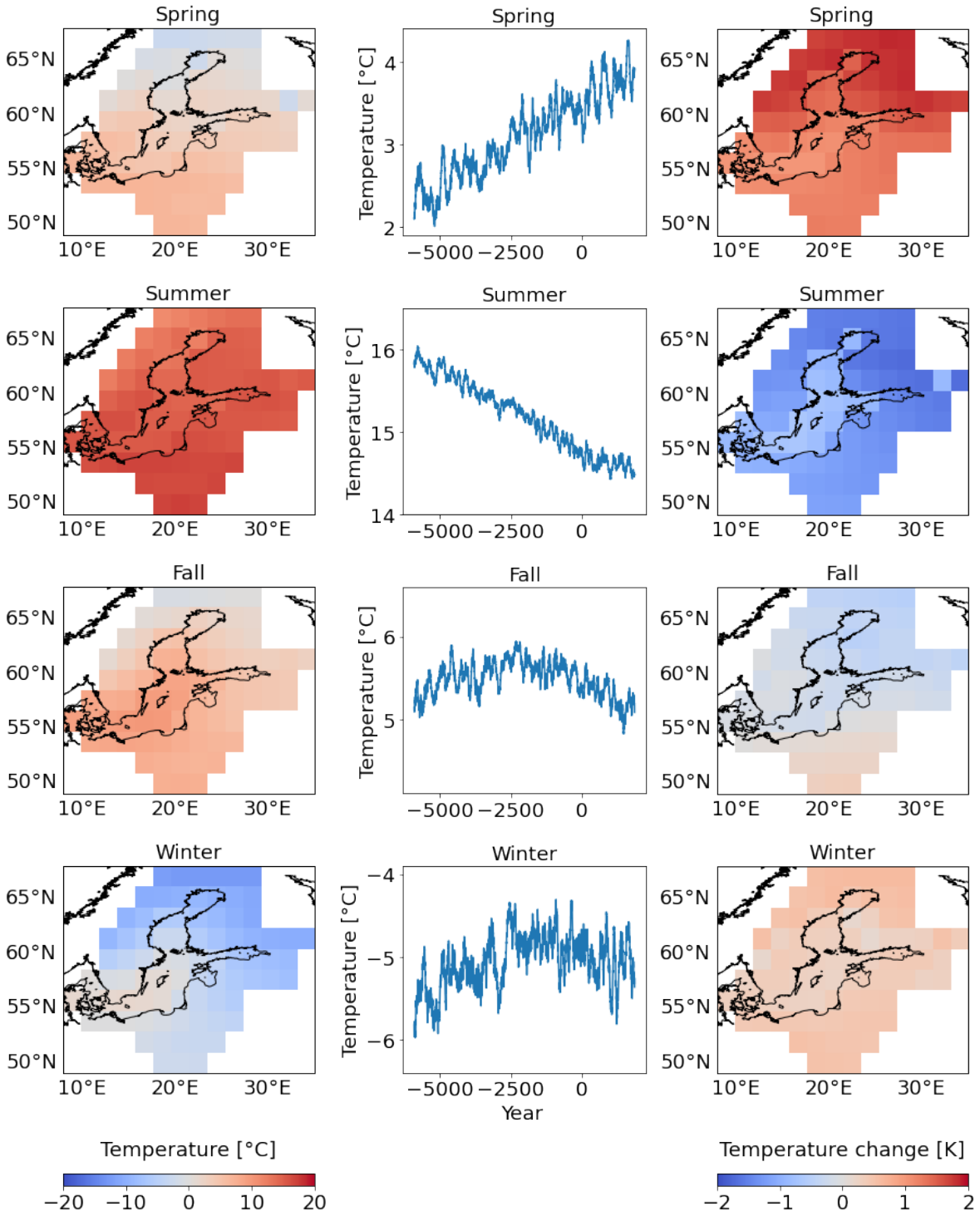

Figure 3.1: The plots in the left column show the Baltic Sea region seasonal temperature averaged over the model period. The central column shows the Baltic Sea region seasonal temperature (100 year MA). In the right column the development of the seasonal temperature over the model period is shown, calculated as the difference of the 1000 year mean temperature of model start and end.

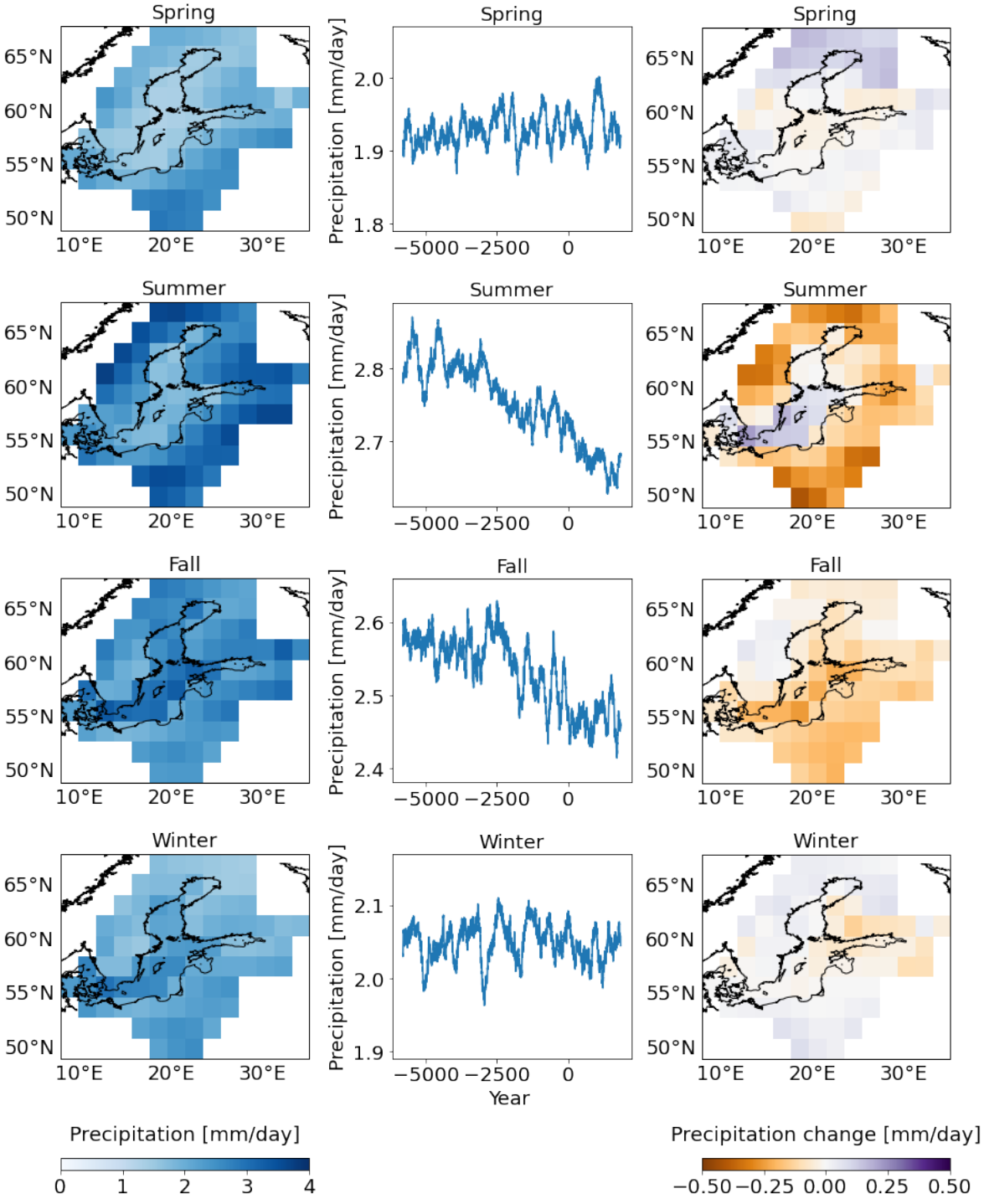

Figure 3.2: The plots in the left column show the Baltic Sea region seasonal precipitation averaged over the model period. The central column shows the Baltic Sea region seasonal precipitation (100 year MA). In the right column the development of the seasonal precipitation over the model period is shown, calculated as the difference of the 1000 year mean precipitation of model start and end.

Most of the map plots in Figure 3.1 and 3.2 show differences in temperature and precipitation between the Baltic Sea itself and land covered area. For the land covered area there are also some differences between the North and South notable. These differences were further investigated dividing the Baltic Sea region into the Baltic Sea itself, land north and land south of 60°N. For these three regions the seasonal temperature and precipitation cycles of start, middle and end (1000 year mean) of the model period were analysed. They are shown in Figure 3.3.
Albeit their different scale the temperature cycles are similarly shaped for all three regions. The regions become similarly warm in summer while it is coldest over the land north of 60°N in January and February. The systematic seasonal shift of cooling summers and warming springs shown in the middle column of Figure 3.1 is distinct. Regarding the whole model period all three regions are cooling from June to September while they become warmer from January to May. The precipitation cycles differ between the regions. The Baltic Sea records the highest precipitation in fall and the lowest in May while the land regions record the lowest precipitation from January to March and the highest in June and July. This pattern sustains over the model period with a general trend of decreasing precipitation in summer and fall which coincides with the findings in Figure 3.2 (middle an right column).

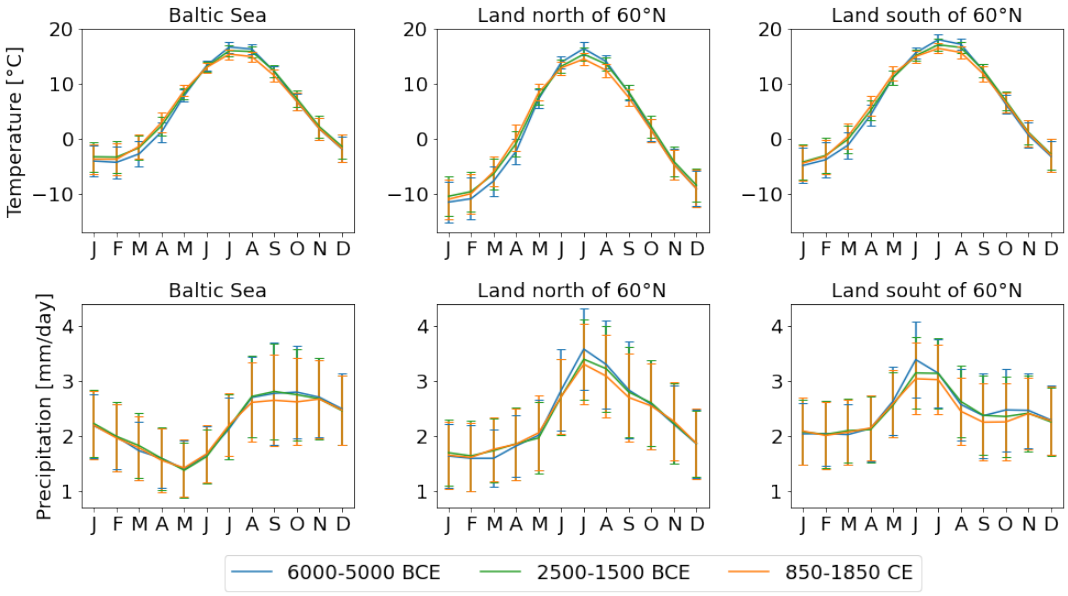

Figure 3.3: Seasonal cycle developments of temperature and precipitation of the Baltic Sea region divided into the Baltic Sea, land north and land south of 60°N. The monthly mean values for 1000 year periods at begin, middle and end of the model period are shown. Note the systematic seasonal shift of the temperature and the different precipitation patterns. The error bars display plus/minus the standard deviation of each month.

The correlation coefficients between temperature and precipitation were calculated seasonally for each Baltic Sea region division. They are shown in Table 3.2. The values indicate a positive correlation for winter, a slightly inverse correlation for summer and no correlation for spring and fall. The summer and winter interrelations are further illustrated in Figure 3.4. It shows scatter-plots of temperature and precipitation of the divided Baltic Sea region. The different alignments of the summer and winter scatter-plots result from the sign of the correlation. The positive correlation is most distinct over the land north of 60°N (0.63) and least distinct above the Baltic Sea (0.47) while the inverse correlation is strongest over the Baltic Sea (-0.36) and weakest over land north of 60°N (-0.34), which is also expressed in the sharpness of the scatter-plots.

Table 3.2.: Seasonal correlation between temperature and precipitation for the whole Baltic Sea region and divisions Baltic Sea, land north and land south of 60°N. Apart from the correlation for fall for land south of 60°N all the correlations are statistically significant with p-values below 0.01.

Correlation (p-value)	Spring	Summer	Fall	Winter
Whole region	0.11 (<0.01)	-0.28 (<0.01)	0.13 (<0.01)	0.58 (<0.01)
Baltic Sea	0.03 (<0.01)	-0.36 (<0.01)	0.10 (<0.01)	0.47 (<0.01)
Land north of 60°N	0.19 (<0.01)	-0.22 (<0.01)	0.30 (<0.01)	0.63 (<0.01)
Land south of 60°N	0.07 (<0.01)	-0.34 (<0.01)	0.01 (>0.05)	0.57 (<0.01)

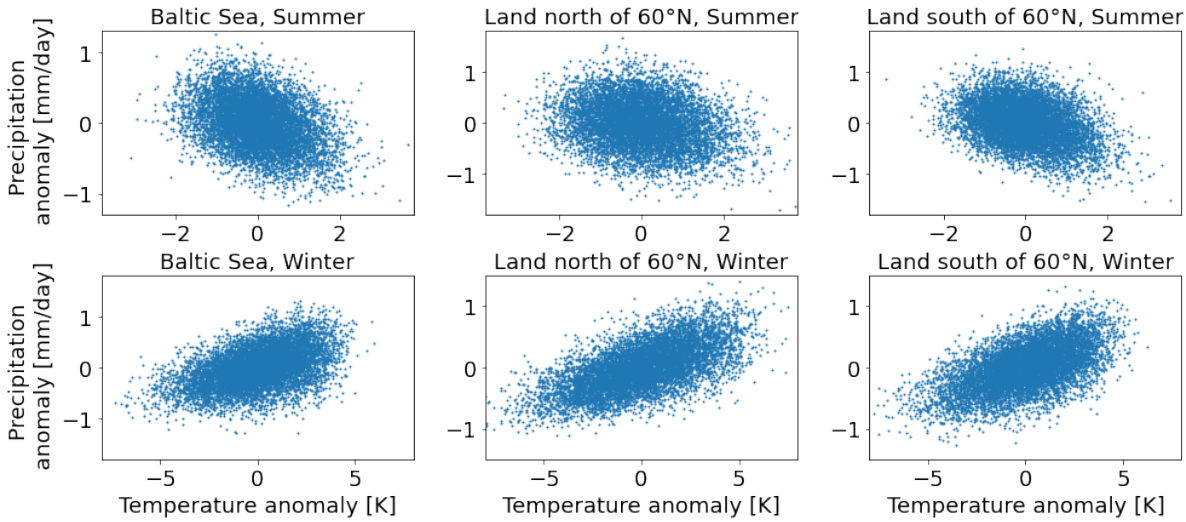

Figure 3.4: Summer and winter interrelation between temperature and precipitation for the divided Baltic Sea region. The data points show precipitation as a function of temperature for summer and winter of each year of the model period.

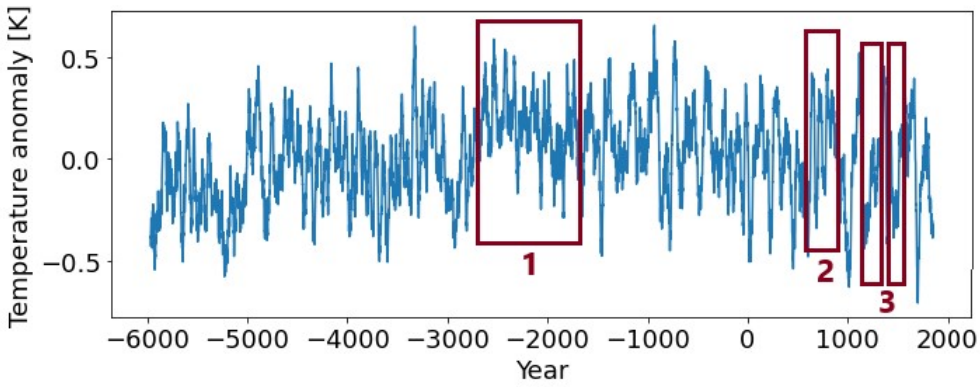

Figure 3.5: Climate periods in the Baltic Sea region temperature. The red squares roughly frame the Holocene Climate Optimum (1), the Medieval Climate Anomaly (2) and the Little Ice Age (3). Note that there are two squares for the latter because two suitable periods were found with a warmer period in between. This graph shows the temperature anomaly with a 35 year MA for illustratory purposes.

The second key area of focus was to search for and to analyse the Baltic Sea region climate during the Holocene Climate Optimum (HCO), the Medieval Climate Anomaly (MCA) and the Little Ice Age (LIA). While Figure 3.5 shows the Baltic sea region temperature anomaly with a 35 year MA, the periods were identified based on the data without MA. Four periods were found that can be interpreted as the climate periods above (framed in Figure 3.5).
The HCO lasted from 2664 to 1567 BCE with a temperature anomaly of +0.17K. The MCA lasted from 604 to 843 CE with a temperature anomaly of +0.16K. For the LIA two periods were considered: the first from 1130 to 1280 CE from now on referred to as LIA1 and the second from 1364 to 1483 CE from now on referred to as LIA2 with temperature anomalies of -0.22K and -0.28K respectively. In contrast the whole period from 1130 to 1483 CE only has a temperature anomaly of -0.14K. Figure 3.6 shows the period anomalies in a spatial resolution in the left column. A strong North to South gradient is visible during the LIA2, while the north was up to 0.5K cooler, the far south was even slightly warmer. During the other three periods the gradient also exists but it is less pronounced. The precipitation anomalies amount to +0.008 mm/day (+0.4%) during the HCO, -0.048 mm/day (-2.1%) during the MCA, -0.043 mm/day (-1.9%) during the LIA1 and -0.023 mm/day (-1.0%) during the LIA2. The highest precipitation occurred in the southwest during the HCO, in the southeast during the LIA1 and in the East during LIA2 (see right column of Figure 3.6). There is no clear precipitation anomaly pattern distinct as the systematic seasonal temperature shift. Table 3.3 summarizes the anomalies during the climate periods.

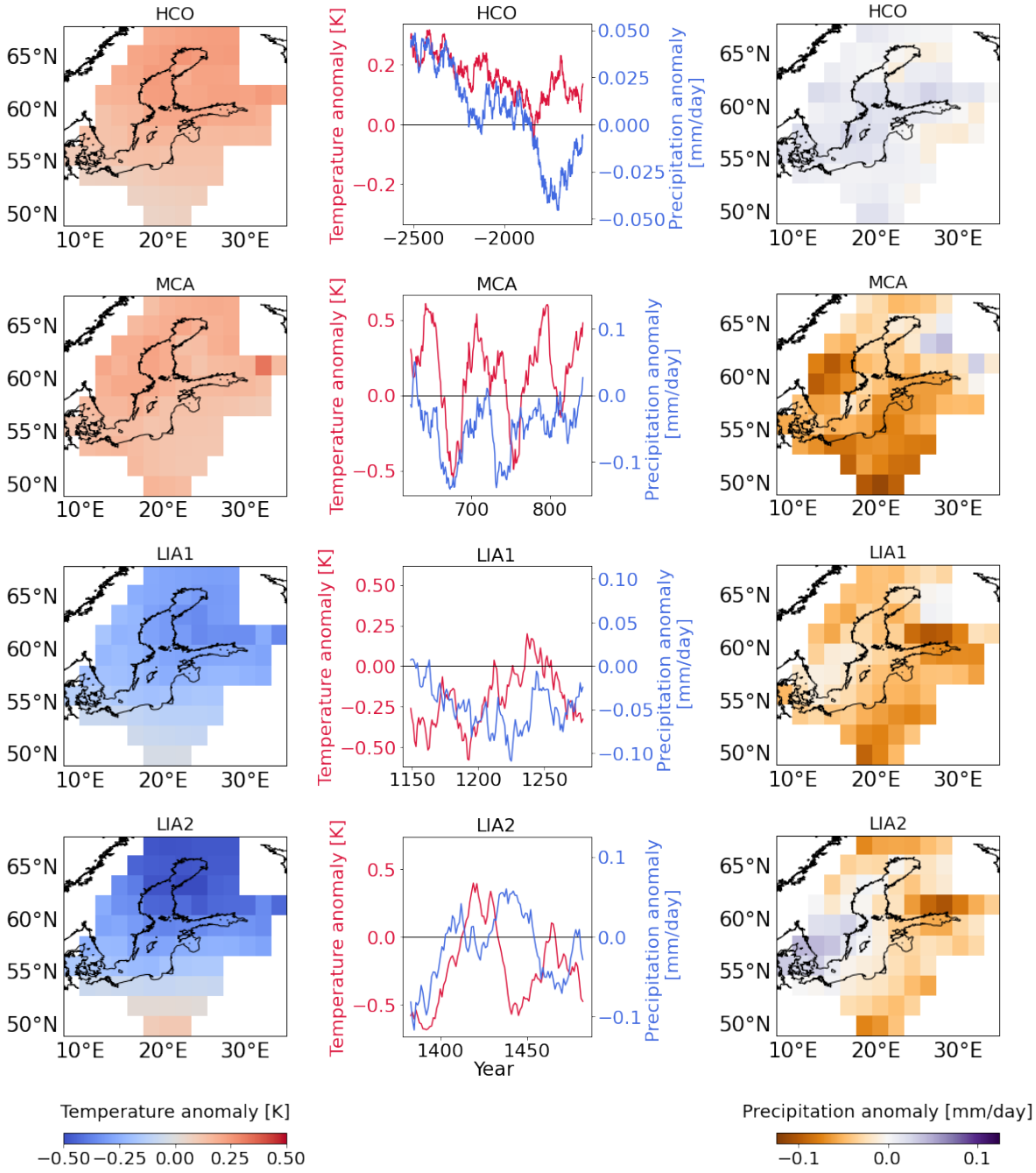

Figure 3.6: Temperature and precipitation anomalies during HCO, MCA, LIA1 and LIA2. The map plots shows the temperature (left column) and precipitation (right column) anomalies from the model mean during the climate periods. In the middle column the anomalies are averaged over the Baltic Sea region thus displayed over the according period, with MAs of 150 years (HCO) and 20 years (others) respectively. Integrating the plots over space and time respectively yields the total anomalies of the periods shown in Table 3.3.

Table 3.3.: Identified climate periods. The duration of the periods and the temperature and precipitation anomalies to the model period mean are shown.

Period	Temperature anomaly [K]	Precipitation anomaly [mm/day]
HCO, 2664-1567 BCE	+0.17	+0.008
MCA, 604-843 CE	+0.16	-0.048
LIA1, 1130-1280 CE	-0.22	-0.043
LIA2, 1364-1483 CE	-0.28	-0.023

Furthermore the seasonal cycles of temperature and precipitation anomalies of the climate periods were analysed. They are shown in Figure 3.7. Figure A.2 shows the same cycles without error bars for a better visibility. In order to maintain some spatial resolution the Baltic Sea region was divided into the usual three parts. The HCO temperature consistently stayed above the model mean with bigger deviations in fall and winter and almost no deviations in spring and summer while the HCO precipitation seasonal cycles move around the model mean with highs in March and September and a low from April to July. The MCA temperature shows a strong positive anomaly from January to May with a maximum of 1.7K on land north of 60°N in April. It shows a negative anomaly from June/July to September/October depending on the region with a maximum of -0.7K on land north of 60°N in July and August. In September the MCA precipitation shows a strong negative anomaly of 10% for the Baltic Sea and 9% for land north of 60°N while the southern land received less precipitation than the model mean almost over the whole year which results in the darkest shade of orange in the precipitation anomaly map plot in Figure 3.6 (right column). LIA1 and LIA2 show similar temperature patterns while the LIA2 is colder in March and April and from August to December and warmer in January and February over the Baltic Sea and the northern land. Over the whole Baltic Sea region the two periods had a positive temperature anomaly from March to May and a negative anomaly from July to February except the LIA2 in January and February over the southern land. The precipitation cycles show negative anomalies in general but no distinct pattern.
In general the temperature and precipitation seasonal cycles of MCA, LIA1 and LIA2 look fairly similar and totally different than the cycles of the HCO. They show a positive temperature anomaly in spring and a negative anomaly in summer and early fall as well as a negative precipitation anomaly from May to October depending on the analysed region.

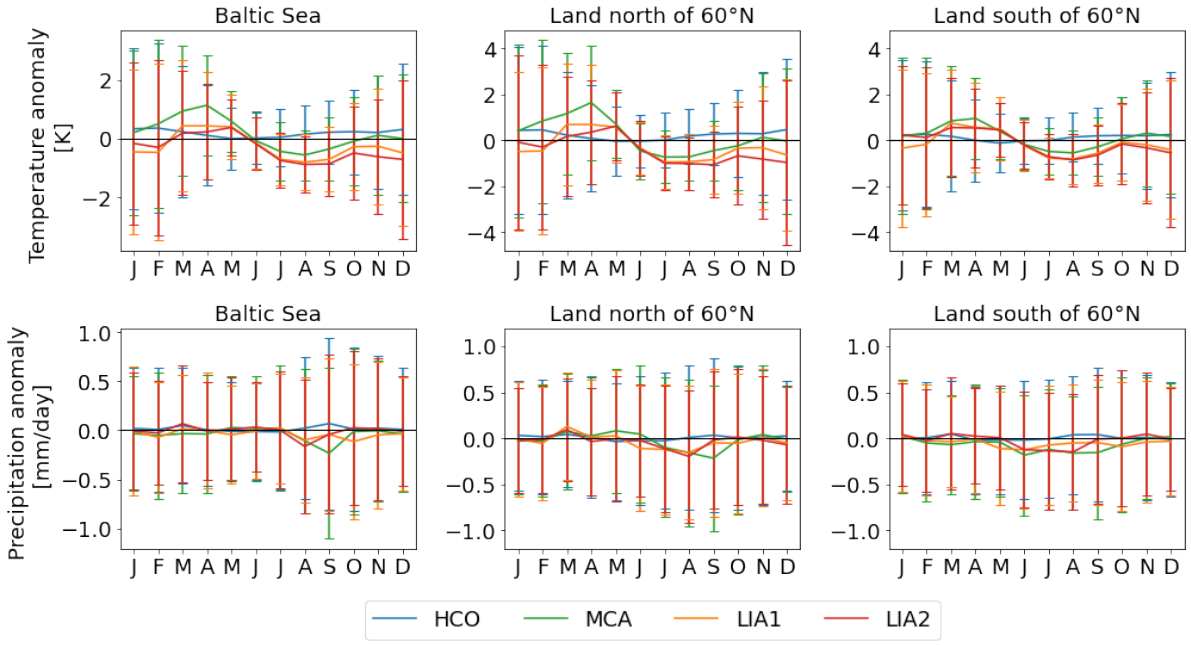

Figure 3.7: Monthly temperature and precipitation anomalies to the model mean during HCO, MCA, LIA1 and LIA2. The Baltic Sea region was divided into Baltic Sea, land north and land south of 60°N again. Integrating the curves over the whole year and the whole region gives the values shown in Table 3.3. As this Figure shows temperature and precipitation anomalies the uncertainty intervals of +/- the standard deviation are large compared to the shown values.

As mentioned before and shown in Table 3.2 a seasonal cycle of temperature-precipitation correlation is distinct in the model data. Albeit some minor deviations in LIA2 January and MCA April and May this pattern persists when the correlation cycle is regarded for the climate periods (see Figure 3.8). The summer correlations lie around -0.3 while the winter correlations amount to between 0.55 and 0.6. Spring and fall act as transitional periods without any notable correlation.

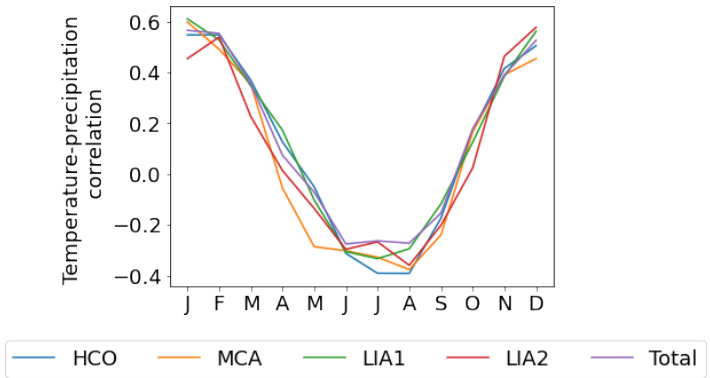

Figure 3.8: Seasonal cycle of temperature-precipitation correlation during the HCO, MCA, LIA1 and LIA2 compared to the model mean called 'Total'.

Apart from 2m temperature and mean precipitation another variable was analysed within this research: The mean sea level pressure. More precisely the pressure difference between the Azores High and the Icelandic Low was calculated (see chapter 2.2.3). On average this difference amounts to 2.1 kPa in spring, 1.8 kPA in summer, 2.2 kPA in fall and 3.2 kPa in winter. The spring pressure difference anomaly from the seasonal model mean, shown in Figure 3.9, increases consistently over the model period while there is a decreasing trend notable for the other three seasons. For the last 2000 years these trends seem to diminish.

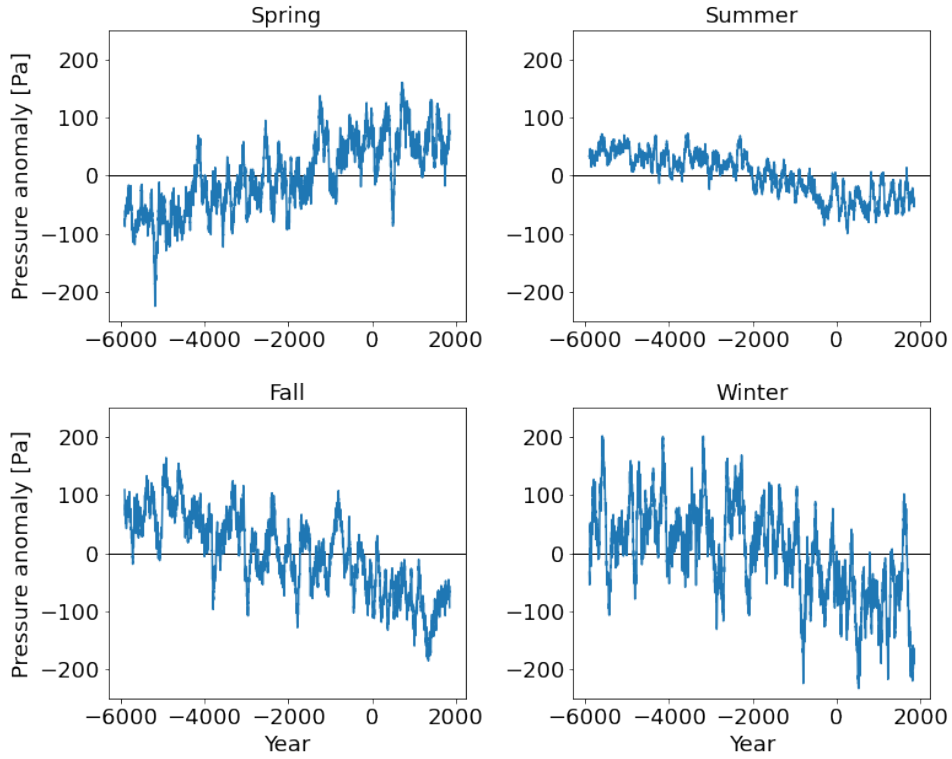

Figure 3.9: Seasonal NAO pressure difference anomaly from seasonal model mean. The curves are smoothed with a 100 year MA. Note how only the spring pressure increase while the other three decrease. Also note that the pressure anomaly in summer is changing on a smaller scale than during the other seasons.

The seasonal Pearson correlation between the described pressure difference and the Baltic Sea region temperature is highest in winter with a value of 0.52, while the correlation in spring, summer and fall amount to 0.32, 0.33 and 0.41 respectively. With the Baltic Sea region precipitation the maximum correlation is 0.28, also in winter, which is the only positive correlation coefficient and also the only correlation with an absolute amount higher than 0.15. All the correlation values are shown in Table 3.4.

Table 3.4.: Seasonal Pearson correlation coefficients between the NAO pressure difference (referred to as pressure) and the Baltic Sea region temperature and precipitation. All of the correlations are statistically significant with p-values below 0.01.

Correlation	Spring	Summer	Fall	Winter
Pressure-temperature	0.32	0.33	0.41	0.52
Pressure-precipitation	-0.06	-0.15	-0.13	0.28

In order to investigate a possible influence of the pressure difference on the previously discussed climate periods, the anomalies of the seasonal pressure difference during these periods from the seasonal mean over the model period were calculated. The values are shown in Table 3.5. The MCA anomaly is the highest in spring (+116 Pa) and even negative during the other seasons. The anomalies during LIA1 and LIA2 are lowest during fall (-136 Pa and -127 Pa) and only positive in spring. The HCO anomaly has a distinctly lower seasonal fluctuation than the anomalies during the other three seasons and it is highest in winter with +46 Pa.
As previously done in Figure 3.8 for the correlation between Baltic Sea region temperature and precipitation, the seasonal cycles of correlation between pressure difference and temperature and precipitation are shown in Figure 3.10. The correlation was observed over the whole model period as well as for the previously discussed climate periods. Generally all seasonal correlation cycles show the same pattern of highest correlation in winter and lowest correlation in summer for both the correlation of pressure difference with temperature and with precipitation of the Baltic . For each period the correlations with temperature are higher than the correlations with precipitation which turn slightly inverse during summer and fall.

Table 3.5.: Seasonal pressure difference anomalies from seasonal model period mean pressure difference between Azores High and Icelandic Low during the climate periods HCO, MCA, LIA1 and LIA2.

Pressure difference anomaly [Pa]	Spring	Summer	Fall	Winter
HCO	-9	12	3	46
MCA	116	-36	-67	-82
LIA1	28	-46	-136	-69
LIA2	58	-55	-127	-90

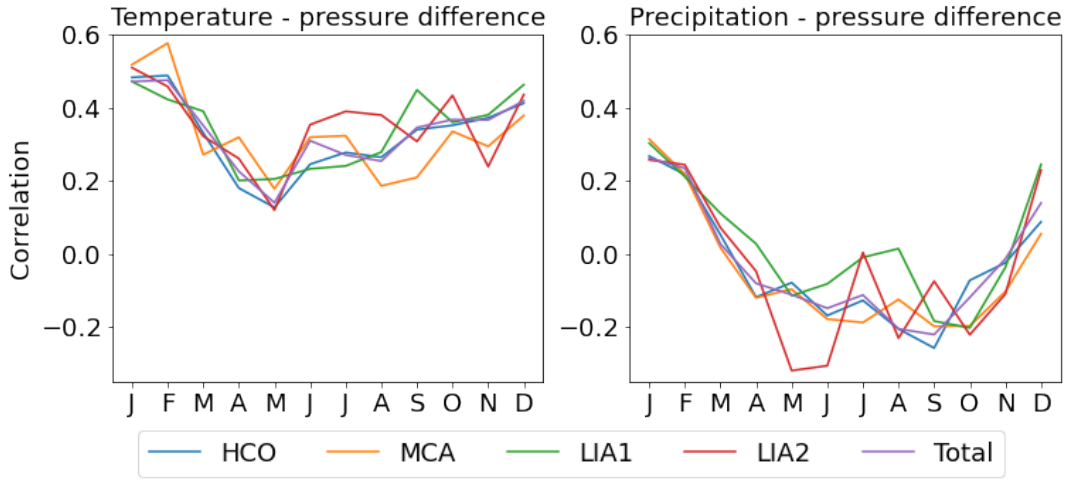

Figure 3.10: Seasonal cycle of the correlations of the pressure difference between Azores High and Icelandic Low and the Baltic Sea region temperature (left) and precipitation(right).

In the end of this research the influence of MA length on the correlation between pairs of Baltic Sea region temperature and precipitation and the pressure difference representing the NAO was analysed. The results are shown in A.3 and A.4.

Chapter 4.

Discussion and Conclusion

In this research the Baltic Sea catchment area, referred to as Baltic Sea region, was characterized by a self-made mask that was used as a whole or divided into the three parts Baltic Sea, land north and land south of 60°N (see Figure 2.2 and 2.3). This description of the region is superior to using a latitude-longitude rectangle. It leaves out the grid points in the northwest over the Norwegian mountains which belong to the Atlantic catchment area. These mountains receive a lot of precipitation which is why the Baltic Sea described by the mask received in comparison 1.5% less precipitation over the model period. The exclusion of northern combined with the inclusion of southern grid points result in the mask region 0.8K being warmer. The precipitation difference varies more significantly over the model period (see Figure A.1), which indicates that the use of the mask had a stronger impact on analysed precipitation developments than on analysed temperature developments.

The analysed data was resolved in 1.875°x1.875°. Albeit a better resolution would allow a more accurate mask of the Baltic Sea catchment area as well as a more accurate division of that mask into areas covered by land or water, it wouldn't have a strong influence on the main findings of this research.

The results of the investigated orbitally driven simulation are impacted by the use of the proleptic Gregorian calendar which stays constant over the whole simulation period. As the Earth's orbital period varies on a small scale the calendrical and the astronomical year are never perfectly aligned [Berger, 1978]. This discrepancy affects the seasons which causes the simulated climate to differ from the actual climate. However these variations are minor and they don't affect the fundamental findings of this research either.

The general seasonal northern hemisphere temperature cycle is distinct in the model data (see Figure 3.1, left column). In the transition from summer to winter the temperature over the Baltic Sea water body lags slightly and stays warmer than over land which can be attributed to the high heat capacity of the water. In accordance with

a north to south increase in insolation there is a north-south temperature gradient visible. Over the model period the spring months are systematically warming while the summer months are cooling (see Figure 3.1 middle column and Figure 3.3 top row). This change is least pronounced over the Baltic Sea and most pronounced in the northern land regions (see Figure 3.1 right column). The systematical shift is caused by orbital parameter changes [Berger, 1978]. Over the whole model period northern hemisphere summer insolation decreases while winter insolation increases [e.g. Wirths et al., 2023]. As the solar influence on the northern hemisphere climate is weakest in winter the influence of increased winter insolation shifts to spring where there solar influence rises again. Consequently this temperature shift can be attributed to the inclusion of solar forcing in the investigated run SLO0043 of the MPI-ESM1.2.

The Baltic Sea region mean precipitation over the model period is higher over land than over the Baltic Sea in spring and summer and vice versa in fall and winter (see Figure 3.2 left column). This is represented in different seasonal precipitation cycles (see 3.3, bottom row) of the areas covered by land and water. The monthly precipitation changes over the model period are small compared to their annual variance shown in the error bars which represent plus/minus the standard deviation. Furthermore Kjellström and Ruosteenoja [2007] found very similar seasonal cycles in a control run of a regional climate model ensemble from 1961 to 1990. Consequently the determination of any systematic precipitation shift over the model period is questionable. This is further affirmed by the findings of Stansell et al. [2017]. For the middle Holocene which comprises the first half of the model period they described a precipitation decrease from November to April (coarsely corresponding to winter, DJF, and spring, MAM, in this research) and/or a precipitation increase from May to October (coarsely corresponding to summer, JJA, and fall, SON, in this research) which is contradictory to winter and spring precipitation staying constant and summer and fall precipitation decreasing (see Figure 3.2, middle column) in the analysed model data.

Based on the Baltic Sea region temperature (see Figure 3.5) Holocene climate periods were identified: The HCO from 2664 to 1567 BCE and the MCA from 604 to 843 CE. For the LIA two possible periods were considered, firstly from 1130 to 1280 CE (LIA1) and secondly from 1364 to 1483 CE (LIA2). As of Warden et al. [2017] the HCO started over 1000 years earlier than concluded in this research with the peak prior to the peak marked with (1) in Figure 3.5. But only the period as chosen here shows a distinct positive temperature anomaly, +0.17K in this case. After the peak the Baltic Sea region temperature declines in accordance with Warden et al. [2017], probably because of the systematic decline in summer insolation already mentioned before. The identified MCA period partially overlaps with the proxy based findings of PAGES 2k Consortium [2013] while the estimate of Mann et al. [2009] starts about 100 years after its end. The MCA is characterized by a temperature anomaly of +0.16K from the model mean. Negative temperature anomalies of -0.22K and -0.28K respectively are identified as the first and second LIA period. The LIA2 lies at the start of the cooling period found by PAGES 2k Consortium [2013] and partly overlaps with the reconstruction of Mann et al. [2009] while the LIA1 period doesn't coincide with either of these estimates. As shown

in Figure 3.6, both LIAs are characterized by a stronger cooling in the higher latitudes while this pattern is more distinct during the LIA2. The identified time periods of HCO, MCA and LIA all differ from the findings of other researches and the common estimates. This is not surprising as the investigated MPI-ESM1.2 run is strongly influenced by the applied forcing agents and starting conditions. It is not even supposed to represent the climate periods perfectly. Furthermore the discovered LIA periods are of questionable nature considering volcanism, which is not included in this model run, being a probable cause (at least partially) of the colder temperatures according to PAGES 2k Consortium [2013] and Miller et al. [2012] besides solar forcing and others. Compared with proxy based temperature reconstructions [PAGES 2k Consortium, 2013, Warden et al., 2017] the temperature anomalies of all of the climate periods are rather small, which is a common result as Luterbacher et al. [2016] found the same discrepancy in a complex comparison of reconstructions and simulations. The difference in the temperature estimates suggests that proxy reconstructions tend to overestimate the temperature variability and/or that climate models aren't properly accounting for internal climate variability and the influence of external forcing changes.
The seasonal cycles of temperature anomalies from the model mean were analysed for the climate periods and shown in Figure 3.7. In general the HCO seasonal temperature cycle is the least volatile while the cycles of the other periods all show the same pattern of positive temperature anomalies during spring and negative anomalies during summer and early fall for all three divisions of the Baltic Sea region (see Figure 3.7). As shown in Figure 3.1 there is a systematic shift of warming spring and cooling summer months over the model period that can be ascribed to a shift in northern hemisphere summer and winter insolation. The HCO lays centrally in the model period so that the systematic shift is averaged out and the temperature doesn't deviate much from the model mean. In contrast the MCA and LIAs are located at the end of the model period where temperature differences from the model mean caused by the seasonal temperature shift are more distinct resulting in warmer spring and colder summer and early fall temperatures compared to the model mean.
While the precipitation during the HCO deviated -0.4% from the model mean the Baltic Sea region experienced 1% more precipitation during the LIA2 and a 2% rise during MCA and LIA1 (see Table 3.3). These precipitation differences as well as the precipitation anomaly seasonal cycles of the climate periods (Figure 3.7 and Figure A.2) can be interpreted similarly to the temperature patterns. In Figure 3.2 a decline of summer and fall precipitation over the model period is visible. While the HCO precipitation anomaly seasonal cycle shows, similar to the temperature anomaly, little volatility the cycles of the MCA and the LIAs show a negative precipitation anomaly from May to October depending on the analysed division of the Baltic Sea region. Again any systematic precipitation shifts over the model period are averaged out for the HCO anomaly resulting in little deviation from the model mean, while the shift to drier summer and fall months is distinct in the other climate periods laying at the end of the model period. In Figure 3.7 the uncertainty intervals of $\pm$ the standard deviation are multiple times larger than the temperature and precipitation anomaly values. This effect appears because the monthly standard deviation of the anomalies is the same as the monthly standard deviation of the temperature and precipitation values themselves

as only the scalar monthly mean value is subtracted.

The interrelation between Baltic Sea region temperature and precipitation was analysed calculating the Pearson correlation coefficient. The analysis of Pearson correlation coefficients does not account for autocorrelation between the variables which inflates the correlations to some extent. Due to the large sample size of 7850 data points the p-values of the correlation are very small indicating a statistical significance for every correlation but one. A systematic positive correlation between Baltic Sea region temperature and precipitation is distinct for winter with a maximum of r=0.63 for land north of 60°N. This relation can be reasoned with the known influence of the NAO on northern European climate during winter [Hurrell, 1995]. A large NAO pressure gradient (NAO+ mode) results in a strong heat and moisture transport from the subtropics to higher latitudes in addition with westerlies deviating the flux in north European direction while a smaller pressure gradient (NAO- mode) implies the weakening of this effect and colder and drier northern European climate [Börgel, 2020]. The lack of positive correlations during other seasons confirms the limitation of the NAO influence to winter months. During summer correlation coefficients of about -0.3 indicate a slightly inverse correlation between temperature and precipitation which could possibly be caused by atmospheric blocking mechanisms [Pfahl and Wernli, 2012] causing a low or high pressure system to station over the Baltic Sea area for a prolonged time period resulting in low temperatures and high precipitation or vice versa.
The seasonal cycle of the Baltic Sea region temperature-precipitation correlation (shown in Figure 3.8) doesn't vary substantially during HCO, MCA or LIA.

Furthermore the pressure difference between Azores High and Icelandic Low was calculated for the model period (further referred to as NAO pressure). Instead of subtracting the stationary pressure values of Lisbon and Reykjavik, each NAO pressure value was calculated as the difference of the minimum pressure inside a box around the Icelandic Low and the maximum pressure inside a box around the Azores High (see 2.2.3 for details). Albeit this approach isn't accurate if the actual maximum or minimum values of the pressure systems momentarily lay outside the boxes it delivers a very good estimate of the NAO pressure.
During winter the NAO pressure amounts to about 3 kPA, during the other seasons to about 2 kPA giving a potential explanation for why the NAO influence on northern European climate is usually limited to winter [Lehmann et al., 2002]. Over the model period fall and winter NAO pressure decrease between 100-200 Pa while the spring pressure shows a similarly scaled increase and the summer pressure doesn't show any significant trend at all (see Figure 3.9).
In order to analyse the influence of the NAO on HCO, MCA and LIA the seasonal NAO pressure anomalies during the climate periods were calculated. These anomalies to the seasonal model mean are influenced by the systematic spring pressure increase and fall and winter pressure decrease over the model period. Taking these trends into account the MCA still experienced higher than average NAO pressure in spring while LIA1 and 2 experienced lower than average NAO pressure in fall (see Table 3.5). Coincidingly the MCA temperature was distinctly higher and the LIA temperatures

distinctly lower during the same time of the year. This connection is in accordance with Trouet et al. [2009] who found strong NAO+ conditions during the MCA and a weakening of those to be an aspect of the transition into the LIA, albeit the findings of this research are limited to the MCA spring and the LIA fall, which might indicate the temporary influence of the NAO on Baltic Sea region climate during seasons other than winter.
The seasonal Pearson correlation of the NAO pressure with the Baltic Sea region temperature is generally higher than with the Baltic Sea region precipitation (see Table 3.4). Both correlations show a similar seasonal cycle with a clear maximum in winter (see Figure 3.10) further confirming the NAOs influence on Baltic Sea region climate during winter. Apart from some unsystematic deviations these cycles remain similarly shaped if the climate periods HCO, MCA and LIA are observed. Consequently no systematic correlation change during the periods can be deduced. As the used Pearson correlation does not account for autocorrelation between the variables all of the correlations are inflated to some degree.

Summing up, the Baltic Sea region experienced a systematic seasonal temperature shift characterized by warming spring and cooling summer months over the model period caused by a shift of northern hemisphere insolation from summer to winter. Furthermore the data suggests summer and fall systematically becoming drier over the model period, but large error intervals and contrary findings of a proxy based research indicate caution. HCO, MCA and LIA were identified with small temperature anomalies of about $\pm$0.2K and during time intervals fairly differing from the estimated periods of other researches. The findings of the LIA have to be questioned in general as the climate period is at least partially affected by volcanic forcing which the model run didn't account for. The influence of the NAO on the climate of the Baltic Sea region during winter is distinct in the model data as strong correlations between temperature and NAO pressure difference as well as precipitation can be found. Additionally significant temperature anomalies during MCA and LIA in spring and fall, respectively, were discovered to coincide with positive and negative, respectively, NAO pressure anomalies during the same seasons.

Appendix A.

Figures

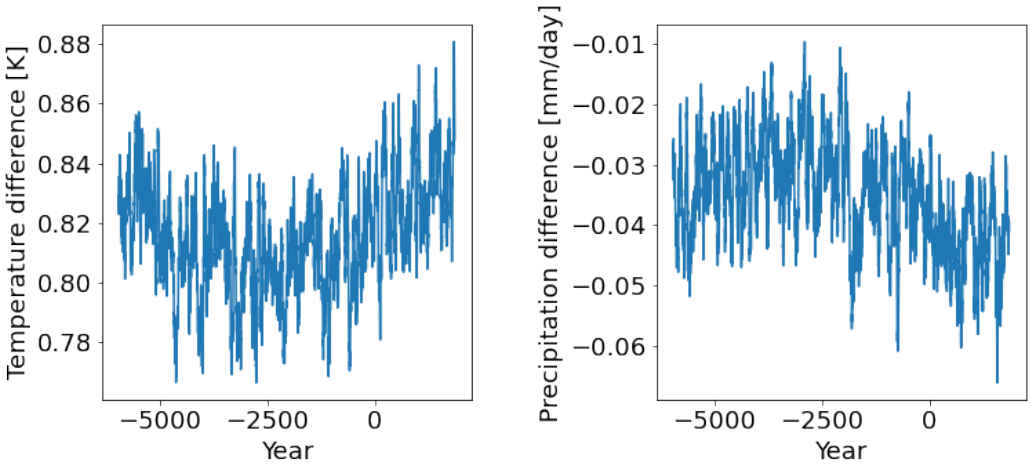

Figure A.1: Difference of the mean temperature (left) and mean precipitation (right) between the two regions used to characterize the Baltic Sea catchment area (see chapter 2.2.1. The 50 year MA is depicted. The temperature via specific mask is about 0.82K higher than the temperature via longitude-latitude rectangle and the precipitation is about 0.035 mm/day (1.5% of model mean) lower on average.

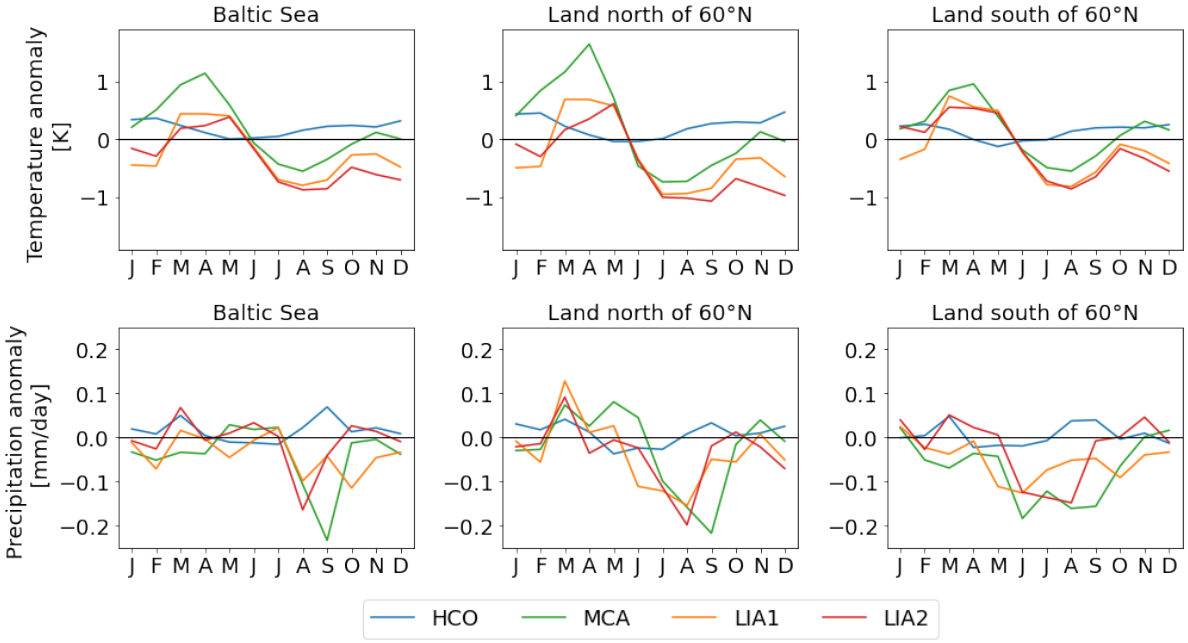

Figure A.2: Annual cycle of temperature and precipitation anomalies to the model mean during HCO, MCA, LIA1 and LIA2. The Baltic Sea region was divided into Baltic Sea, land north and land south of 60°N. This Figure doesn't show error bars for a better visibility.

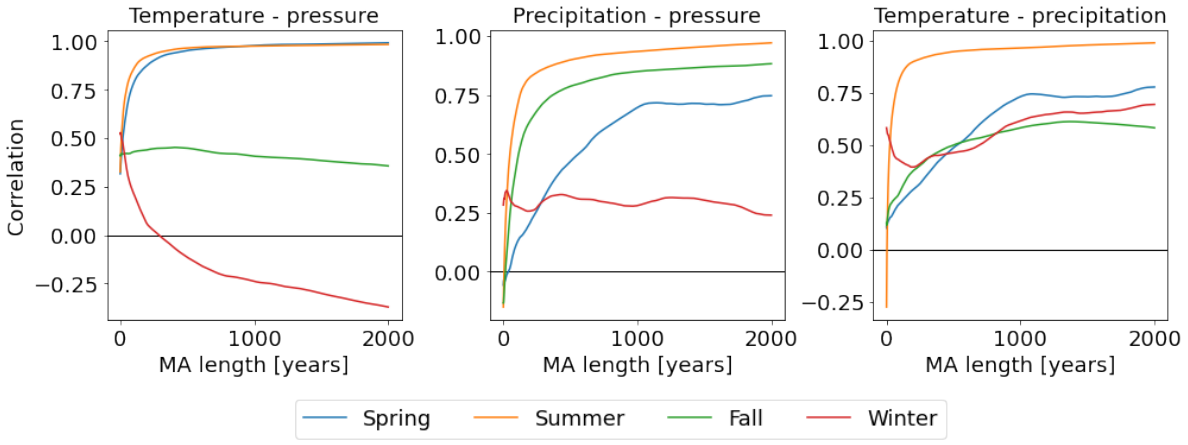

Figure A.3: Seasonal correlation of pairs of Baltic Sea region temperature and precipitation and the pressure difference representing the NAO, shown as a function of moving average length used to smooth the data. Note how some correlations converge to 1 while others show a totally different behaviour.

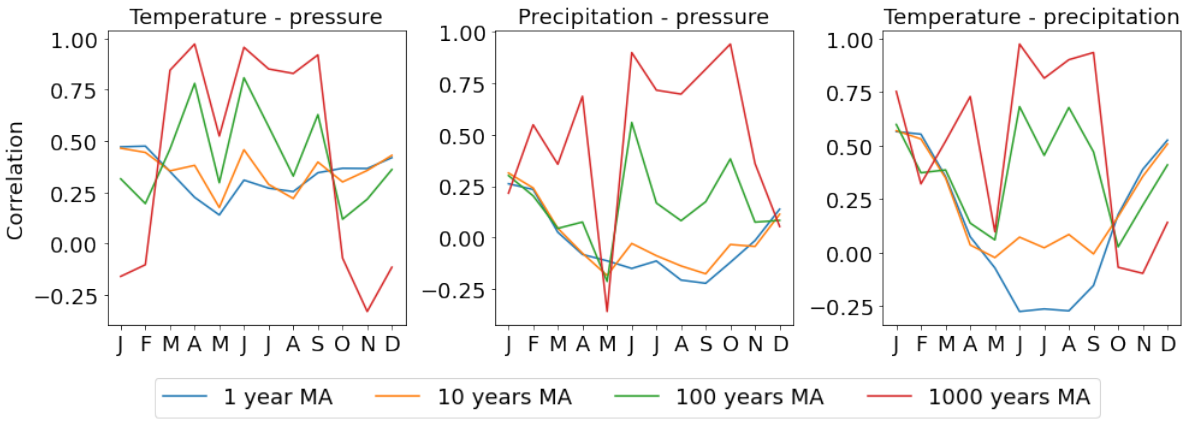

Figure A.4: Seasonal correlation cycle of pairs of Baltic Sea region temperature and precipitation and the pressure difference representing the NAO. The data sets are smoothed with no (1 year), a 10, 100 and 1000 year MA. Note how the correlation patterns inverse from higher correlation in winter and lower in summer to higher correlation in summer and lower in winter with rising MA lengths. Also note the anomaly in May for all three correlations, most distinct for the precipitation-pressure correlation.

Bibliography

PAGES 2k Consortium. Continental-scale temperature variability during the past two millennia. *Nature Geoscience*, 6:339–346, 2013. https://doi.org/10.1038/ngeo1834.

P. Ludwig, J. J. Gómez-Navarro, J. G. Pinto, C. C. Raible, S. Wagner, and E. Zorita. Perspectives of regional paleoclimate modeling. *Annals of the New York Academy of Sciences*, 1436(1):54–69, 2018. https://doi.org/10.1111/nyas.13865.

T. G. Askjær, Q Zhang, F. Schenk, F. C. Ljungqvist, Z. Lu, et al. Multi-centennial Holocene climate variability in proxy records and transient model simulations. *Quaternary Science Reviews*, 296:107801, 2022. https://doi.org/10.1016/j.quascirev.2022.107801.

M. A. Giorgetta, J. Jungclaus, C. H. Reick, S. Legutke, J. Bader, et al. Climate and carbon cycle changes from 1850 to 2100 in MPI-ESM simulations for the Coupled Model Intercomparison Project phase 5. *Journal of Advances in Modeling Earth Systems*, 5: 572–597, 2013. https://doi.org/10.1002/jame.20038.

V. Balaji, F. Couvreux, J. Deshayes, J. Gautrais, F. Hourdin, and C. Rio. Are general circulation models obsolete? *Proceedings of the National Academy of Sciences USA*, 119(47):e2202075119, 2022. https://doi.org/10.1073/pnas.2202075119.

B. Stevens, M. Giorgetta, M. Esch, T. Mauritsen, T. Crueger, et al. Atmospheric component of the MPI-M Earth System Model: ECHAM6. *Journal of Advances in Modeling Earth Systems*, 5:146–172, 2013. https://doi.org/10.1002/jame.20015.

J. H. Jungclaus, N. Fischer, H. Haak, K. Lohmann, J. Marotzke, et al. Characteristics of the Ocean Simulations in the Max Planck Institute Ocean Model (MPIOM) the Ocean Component of the MPI-Earth System Model. *Journal of Advances in Modeling Earth Systems*, 5:422–446, 2013. https://doi.org/10.1002/jame.20023.

C. H. Reick, T. Raddatz, V. Brovkin, and V. Gayler. Representation of natural and anthropogenic land cover change in MPI-ESM. *Journal of Advances in Modeling Earth Systems*, 5:459–482, 2013. https://doi.org/10.1002/jame.20022.

O. Gutjahr, D. Putrasahan, K Lohmann, J. H. Jungclaus, J.-S. von Storch, et al. Max Planck Institute Earth System Model (MPI-ESM1.2) for the High-Resolution Model Intercomparison Project (HighResMIP). *Geoscientific Model Development*, 12:3241–3281, 2019. https://doi.org/10.5194/gmd-12-3241-2019.

J. Bader, J. Jungclaus, N. Krivova, S. Lorenz, A. Maycock, et al. Global temperature modes shed light on the Holocene temperature conundrum. *Nature Communications*, 11(4726), 2020. https://doi.org/10.1038/s41467-020-18478-6.

A. Dallmeyer, M. Claussen, S. J. Lorenz, and T. Shanahan. The end of the African humid period as seen by a transient comprehensive Earth system model simulation of the last 8000 years. *Climate of the Past*, 16(1):117–140, 2020. https://doi.org/10.5194/cp-16-117-2020.

S.-K. Min, S. Legutke, A. Hense, and W.-T. Kwon. Climatology and Internal Variability in a 1000-Year Control Simulation with the Coupled Climate Model ECHO-G. Technical Report 2, 2004. Max Planck Institute for Meteorology, Hamburg, Germany. https://www.researchgate.net/publication/235703695_Climatology_and_internal_variability_in_a_1000-year_control_simulation_with_the_coupled_climate_model_ECHO-G.

J. H. Jungclaus, N. Keenlyside, M. Botzet, H. Haak, J.J. Luo, et al. Ocean Circulation and Tropical Variability in the Coupled Model ECHAM5/MPI-OM. *Journal of Climate*, 19(16):3952–3972, 2006. https://doi.org/10.1175/JCLI3827.1.

J. H. Jungclaus, S. J. Lorenz, C. Timmrech, C. H. Reick, V. Brovkin, et al. Climate and carbon-cycle variability over the last millennium. *Climate of the Past*, 6:723–737, 2010. https://doi.org/10.5194/cp-6-723-2010.

X. Shi, G. Lohmann, D. Sidorenko, and H. Yang. Early-Holocene simulations using different forcings and resolutions in AWI-ESM. *The Holocene*, 30(7):996–1015, 2020. https://doi.org/10.1177/0959683620908634.

Q. Zhang, E. Berntell, J. Axelsson, J. Chen, Z. Han, et al. Simulating the mid-Holocene, last interglacial and mid-Pliocene climate with EC-Earth3-LR. *Geoscientific Model Development*, 14(2):1147–1169, 2021. https://doi.org/10.5194/

gmd-14-1147-2021.

P. Hopcroft and P. J. Valdes. Paleoclimate-conditioning reveals a North Africa land–atmosphere tipping point. *Proceedings of the National Academy of Sciences USA*, 118(45):e2108783118, 2021. https://doi.org/10.1073/pnas.2108783118.

P. Braconnot, D. Zhu, O. Marti, and J. Servonnat. Strengths and challenges for transient Mid- to Late Holocene simulations with dynamical vegetation. *Climate of the Past*, 15 (3):997–1024, 2019. https://doi.org/10.5194/cp-15-997-2019.

W. Sun, J. Liu, L. Wan, L. Ning, and M. Yan. Simulation of northern hemisphere mid-latitude precipitation response to different external forcings during the Holocene. *Quaternary Science Reviews*, 40(6):1588–1596, 2020. https://doi.org/10.11928/j.issn.1001-7410.2020.06.18.

M. Sigl, M. Winstrup, J. R. McConnell, K. C. Welten, G Plunkett, et al. Timing and climate forcing of volcanic eruptions for the past 2,500 years. *Nature*, 523:543–549, 2015. https://doi.org/10.1038/nature14565.

J. Lin, A. Svensson, C. S. Hvidberg, J. Lohmann, S. Kristiansen, et al. Magnitude, frequency and climate forcing of global volcanism during the last glacial period as seen in Greenland and Antarctic ice cores (60-9 ka). *Climate of the Past*, 18:485–506, 2022. https://doi.org/10.5194/cp-18-485-2022.

M. E. Mann, B. A. Steinman, D. J. Brouilette, and S. K. Miller. Multidecadal climate oscillations during the past millennium driven by volcanic forcing. *Science*, 371: 1014–1019, 2021. https://doi.org/10.1126/science.abc5810.

F. Börgel, C. Frauen, T. Neumann, S. Schimanke, and H. E. M. Meier. Impact of the Atlantic Multidecadal Oscillation on Baltic Sea Variability. *Geophysical Research Letters*, 45, 2018. https://doi.org/10.1029/2018GL078943.

V. Eyring, S. Bony, G. A. Meehl, C. A. Senior, B. Stevens, et al. Overview of the Coupled Model Intercomparison Project Phase 6 (CMIP6) experimental design and organization. *Geoscientific Model Development*, 9:1937–1958, 2016. https://doi.org/10.5194/gmd-9-1937-2016.

M. Kageyama, P. Braconnot, S. P. Harrison, A. M. Haywood, Jungclaus J. H., et al. The PMIP4 contribution to CMIP6 – Part 1: Overview and over-arching analysis plan. *Geoscientific Model Development*, 11:1033–1057, 2018. https://doi.org/10.5194/gmd-11-1033-2018.

B. L. Otto-Bliesner, P Braconnot, S. P. Harrison, D. J. Lunt, A Abe-Ouchi, et al. The PMIP4 contribution to CMIP6 – Part 2: Two interglacials, scientific objective and experimental design for Holocene and Last Interglacial simulations. *Geoscientific Model Development*, 10:3979–4003, 2017. https://doi.org/10.5194/gmd-10-3979-2017.

S. Schimanke, H. E. M. Meier, E. Kjellström, G. Strandberg, and R. Hordoir. The climate in the baltic sea region during the last millennium simulated with a regional climate model. *Climate of the Past*, 8:1419–1433, 2012. https://doi.org/10.5194/cp-8-1419-2012.

E. Kjellström and K. Ruosteenoja. Present-day and future precipitation in the Baltic Sea region as simulated in a suite of regional climate models. *Climatic Change*, 81: 281–291, 2007. https://doi.org/10.1007/s10584-006-9219-y.

F. Börgel. *Long-term Climate Variability of the Baltic Sea Region*. PhD thesis, University of Rostock, Germany, 2020. https://doi.org/10.18453/rosdok_id00002798.

J. W. Hurrell. Decadal Trends in the North Atlantic Oscillation: Regional temperatures and precipitation. *Science*, 269:676–679, 1995. https://doi.org/10.1126/science.269.5224.676.

A. Lehmann, W. Krauss, and H.-H. Hinrichsen. Effects of remote and local atmospheric forcing on circulation and upwelling in the Baltic Sea. *Tellus A: Dynamic Meteorology and Oceanography*, 54(3):299–316, 2002. https://doi.org/10.3402/tellusa.v54i3.12138.

L. Warden, M. Moros, T. Neumann, S. Shennan, A. Timpson, et al. Climate induced human demographic and cultural change in northern europe during the mid-holocene. *Scientific Reports*, 7:15251, 2017. https://doi.org/10.1038/s41598-017-14353-5.

M. E. Mann, Z. Zhang, S. Rutherford, R. S. Bradley, and M. K. Hughes. Global signatures and dynamical origins of the little ice age and medieval climate anomaly. *Science*, 326(5957):1256–1260, 2009. https://doi.org/10.1126/science.1177303.

G. H. Miller, Á. Geirsdóttir, Y. Zhong, D. J. Larsen, and B. L. Otto-Bliesner. Abrupt onset of the Little Ice Age triggered by volcanism and sustained by sea-ice/ocean feedbacks. *Geophysical Research Letters*, 39(2), 2012. https://doi.org/10.1029/2011GL050168.

V. Trouet, J. Esper, N. E. Graham, A. Baker, J. D. Scourse, and D. C. Frank. Persistent positive North Atlantic oscillation mode dominated the Medieval Climate Anomaly.

Science, 3;324(5923):78–80, 2009. https://doi.org/10.1126/science.1166349.

G. C. Hurtt, L. P. Chini, S. Frolking, R. A. Betts, J. Feddema, et al. Harmonization of land-use scenarios for the period 1500-2100: 600 years of global gridded annual land-use transitions, wood harvest, and resulting secondary lands. *Climatic Change*, 109(117), 2011. https://doi.org/10.1007/s10584-011-0153-2.

A. L. Berger. Long-Term Variations of Daily Insolation and Quaternary Climatic Changes. *Journal of the Atmospheric Sciences*, 35(12):2362–2367, 1978. https://doi.org/10.1175/1520-0469(1978)035<2362:LTVODI>2.0.CO;2.

K. Kuliński, G. Rehder, E. Asmala, A. Bartosova, J. Carstensen, et al. Biogeochemical functioning of the Baltic Sea. *Earth System Dynamics*, 13:633–685, 2022. https://doi.org/10.5194/esd-13-633-2022.

C. Wirths, E. Ziegler, and K. Rehfeld. Exploring Holocene temperature trends and a potential summer bias in simulations and reconstructions. Preprint, 2023. Discussion started: 20 February 2023. https://doi.org/10.5194/egusphere-2023-86.

N. D. Stansell, E. S Klein, M. S. Finkenbinder, C. S. Fortney, J. P. Dodd, et al. A stable isotope record of Holocene precipitation dynamics in the Baltic region from Lake Nuudsaku, Estonia. *Quaternary Science Reviews*, 175:73–84, 2017. https://doi.org/10.1016/j.quascirev.2017.09.013.

J. Luterbacher, J. P. Werner, J. E. Smerdon, L. Fernández-Donado, F. J. González-Rouco, et al. European summer temperatures since Roman times. *Environmental Research Letters*, 11(2):024001, 2016. https://doi.org/10.1088/1748-9326/11/2/024001.

S. Pfahl and H. Wernli. Quantifying the relevance of atmospheric blocking for co-located temperature extremes in the Northern Hemisphere on (sub-)daily time scales. *Geophysical Research Letters*, 39(12):L12807, 2012. https://doi.org/10.1029/2012GL052261.

Code availability

The full code used in this research, consisting of 14 Jupyter Notebooks using Python as programming language, is publicly available on `https://github.com/martiwolff/Bachelors-thesis`.

Selbstständigkeitserklärung

Ich versichere hiermit, dass ich die vorliegende Arbeit selbstständig verfasst und keine anderen als die angegebenen Quellen und Hilfsmittel benutzt habe. Ich versichere, dass die eingereichte elektronische Fassung mit den gedruckten Exemplaren übereinstimmt.

Rostock, (Datum)